Available online at www.sciencedirect.com
SCIENCE DIRECT®
Acta Materialia 52 (2004) 3151–3159
Acta MATERIALIA
www.actamat-journals.com

Buckle delamination on patterned substrates

M.-W. Moon [a], K.-R. Lee [b], K.H. Oh [a], J.W. Hutchinson [c,*]

[a] School of Materials Science and Engineering, Seoul National University, Seoul 151-742, Republic of Korea
[b] Future Technology Research Division, Korea Institute of Science and Technology, Seoul 130-650, Republic of Korea
[c] Division of Engineering and Applied Sciences, Harvard University, 29 Oxford St., Cambridge, MA 02138, USA

Received 30 January 2004; received in revised form 10 March 2004; accepted 12 March 2004
Available online 9 April 2004

Abstract

Lithographic techniques applied to a substrate prior to film deposition can create areas of low interface adhesion surrounded by regions of high adhesion. If the film is under compression and if buckle delamination is nucleated, conditions can be controlled such that delaminations are confined to the patterned areas of low adhesion. When the area of low adhesion is a strip, the width of the strip controls the buckle morphology: smooth Euler buckles for narrow strips, asymmetric telephone cord buckles for wider strips, and symmetric varicose buckles under a very limited range of conditions. Results for the elastic energy in the buckled state show that above a critical stress the telephone cord morphology is the preferred morphology. Energy release rates for propagating delaminations are determined for each of the three morphologies. Tapered strips provide an accurate means of measuring interface adhesion based on the width of the strip where the delamination arrests.

Keywords: Films; Buckling; Adhesion; Lithography; Interface toughness

1. Introduction

In addition to its practical importance as a dominant failure mode of thin compressed films, buckle delamination has been a focus of attention because of the intriguing blister shapes that are commonly observed. For a film deposited on a substrate under conditions of equibiaxial compression, the film either fully adheres or fully delaminates under most circumstances. However, depending on factors such as the film stress, thickness and interface adhesion, buckle delaminations can localize and propagate across the film in one of two morphologies: the telephone core buckle or the straight-sided buckle [1–4]. The telephone cord is by far the more common of the two morphologies. Conditions under which each of the two morphologies is expected to occur have been analyzed by Moon et al. [3] and explored experimentally by Volansky [5]. Details of shape and size depend in a complicated way on the factors noted above. Most importantly, their existence depends on interface toughness that increases as the mode mix acting on the interface ahead of the delamination crack shifts from mode I (normal stress) towards mode II (shear stress).

Pre-patterned regions of low adhesion at the interface between the film and substrate constrain the delamination path and thereby give rise to more predictable behavior. When the regions of low adhesion are strips, as in Fig. 1, delaminations, once nucleated, propagate the full length of the strips if the strips are above a critical width. For reasons detailed below, the Euler mode emerges for the narrow strips while a morphology much like the telephone cord mode is preferred for the wider strips. In Fig. 1, buckle delaminations have been nucleated at the wide delaminated region at top of the narrow strips of low adhesion and then have propagated from the top towards the bottom of the figure. As noted in Fig. 1, there are several strips that are too narrow for buckling delamination to occur, i.e. those having $2b \leqslant 6$ μm.

Both the Euler mode and a mode similar to telephone cord mode are in evidence in Fig. 2 where the patterned

* Corresponding author. Tel.: +1-617-495-2848; fax: +1-617-496-0601.
E-mail address: hutchinson@husm.harvard.edu (J.W. Hutchinson).

1359-6454/$30.00 © 2004 Acta Materialia Inc. Published by Elsevier Ltd. All rights reserved.
doi:10.1016/j.actamat.2004.03.014

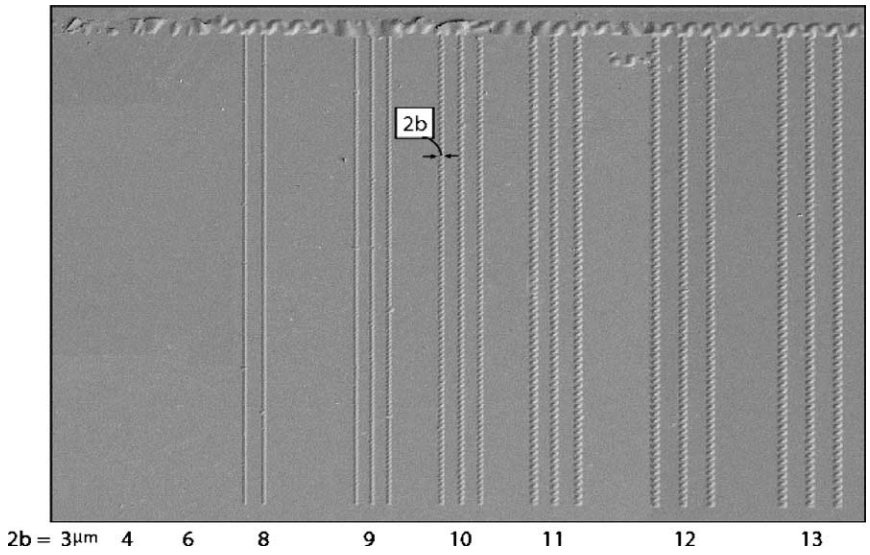

Fig. 1. Buckle delamination along patterned strips of low adhesion between a DLC film and a silicon substrate showing the telephone cord morphology for wider strips and the Euler mode for narrower strips. Delaminations are nucleated in each strip at the top where it joins the wide horizontal strip of low adhesion (whose delamination is nucleated by a indenter). Delaminations propagate from top to bottom. Although not apparent, there are several strips too narrow to allow buckle propagation (those with $2b \leqslant 6$ μm). Delamination was not nucleated in one of the three strips with $2b = 8$ μm. Film properties are given in (11).

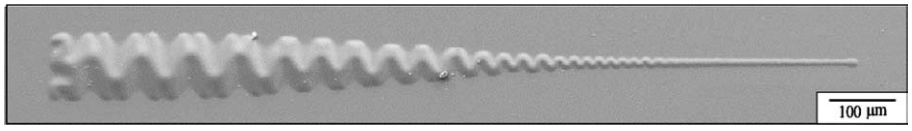

Fig. 2. A buckle delamination that has propagated along a tapered strip of low interface adhesion between a DLC film and a silicon substrate. The telephone cord morphology is evident when the strip is wide but it transitions to the Euler mode when the strip is narrow. The delamination is initiated at the wide end and arrests when the width of the strip drops below a critical width, as discussed in the paper. Film properties are given in (11).

region of low adhesion is a tapered strip. The delamination has been nucleated at the wide end of the strip and has propagated toward the narrow end where it transitions to the Euler mode. While some features of the constrained mode depart from those of a unconstrained telephone cord (e.g. the small nodular regions on the edges of the buckle at the left in Fig. 2), in most respects the two modes are remarkably similar and term telephone cord mode will be used here to characterize the unsymmetric undulating mode. Another notable feature seen in Fig. 2 is the arrest of the buckle delamination at a point where its width becomes too narrow to release sufficient energy to overcome the interface toughness. This feature allows for accurate measurement of interface toughness under conditions relevant to delamination, as will be discussed in the body of the paper.

In this paper the process for patterning regions of low adhesion by lithographic means is discussed for diamond-like-carbon (DLC) films deposited on silicon wafer substrates. Selected experimental observations of buckle delamination of patterned regions of low adhesion are reported for this system. Analyses related to the observations are performed with emphasis on: (1) the relationship among film stress, delamination width and blister morphology as determined by energy in the buckled state, (2) the energy release rate for each of the morphologies, and (3) delamination arrest and its use to determine interface toughness. Potential applications of controlled buckle delamination will also be discussed.

2. Method for creating areas of low interface adhesion

The experimental procedure for patterning regions of low adhesion surrounded by regions of higher adhesion for DLC films on Silicon substrates is briefly addressed with the aid of the schematic in Fig. 3. A 3 nm layer of Al_2O_3 between the Si and the DLC is used to create the regions of low adhesion. This layer is absent in regions of higher adhesion. The first step in creating the Al_2O_3 layer is to use E-beam lithography to expose the desired low adhesion pattern on the substrate (see Fig. 3). Standard lithography tech-

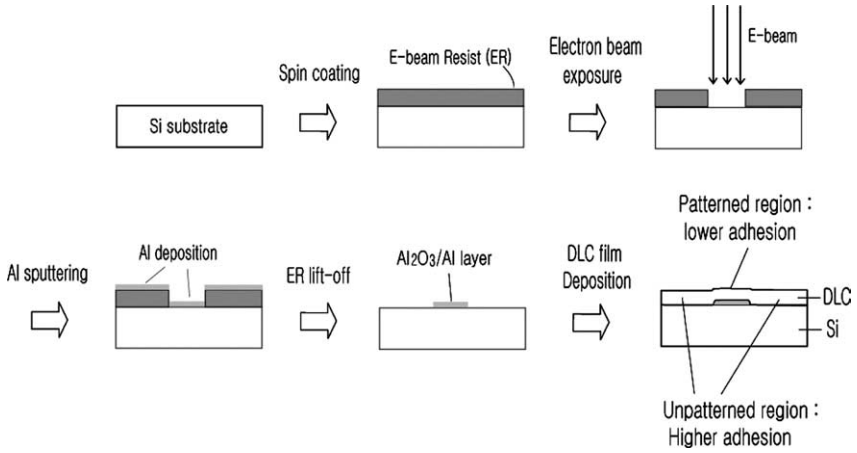

Fig. 3. Schematic for creating patterns of low adhesion.

niques in a clean room environment were employed. The positive E-beam resist (ER) layer was spin-coated on Si (1 0 0) followed by E-beam exposure of the regions selected for low adhesion. A very thin layer of Al is then sputter deposited which, upon oxidation, becomes a Al_2O_3 layer about 3 nm in thickness covering low adhesion regions. The ER layer covering the regions designated to have higher adhesion is removed with acetone and alcohol. The DLC layer is then deposited by the method of PECVD using a *capacitively-coupled r.f.* glow discharge, choosing conditions that from prior experience will lead to buckle delamination. The gas phases are CH_4 and C_6H_6 plus N_2, at a pressure of 1.33 Pa with deposition time ranging from two to seven minutes resulting in DLC film thickness of 0.2–0.82 μm having residual compression between about 0.9 and 2 GPa in the equi-biaxial state [3,6]. Although no direct observation of the location of the interface crack has been made, we believe separation occurs either within Al_2O_3 layer or at the interface between the Al_2O_3 and the DLC. The precise location of the interface crack is not a critical issue for the purposes of this study.

Film stresses and buckle geometries were determined using standard curvature measurement techniques and atomic force microscopy (AFM, AutoProbe CP Research sys.), respectively [6]. The elastic modulus and the Poisson's ratio of the DLC layer under present deposition conditions have been measured using techniques described in [7].

3. Buckle delamination confined to thin strips of constant width

Confinement of a delamination buckle to a narrow strip of low adhesion predetermines the width of the buckle and thereby eliminates the complicated role played by the mode dependence of the interface toughness in setting the buckle width for an unconfined delamination. The buckling and post-buckling behavior of a film under equi-biaxial compression that is detached from a substrate over a strip of width $2b$ is usually modeled as a plate of the same width that is fully clamped along its edges (Fig. 4). This is an excellent approximation for determining the critical stress, buckling amplitude and relevant energy release rates as long as the Young's modulus of the substrate is not less than about one fifth of that of the film [8,9], as will be assumed here. When the substrate has a very low modulus compared to that of the film, deformation of the substrate along the edge of the detached region becomes important such that the assumption of a clamped edge overestimates the constraint.

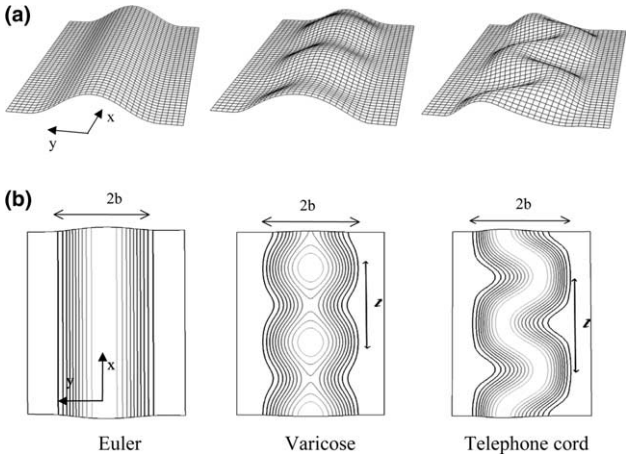

Fig. 4. Geometry and finite element mesh for buckling analysis of a constant width plate (film) clamped along its edges at $y = \pm b$ to a rigid substrate. The Euler mode, the varicose mode and the telephone core mode are depicted in two views.

3.1. Post-buckling energy and energy release rate for the Euler mode

Various aspects of the buckling and post-buckling behavior of infinite long plates subject to equi-biaxial compressive stress that are clamped along their straight edges have been investigated for the purpose of illuminating buckle delamination [10–14]. The mode that governs at the onset of buckling is referred to as the Euler mode (Fig. 4). It is independent of the coordinate x parallel to the strip. The critical compressive biaxial stress at the onset of buckling, σ_C, and the associated normal displacement of the buckling mode, w, are

$$\sigma_C = \frac{\pi^2}{12}\frac{E}{1-v^2}\left(\frac{h}{b}\right)^2, \tag{1}$$

$$w = \frac{\xi h}{2}\left(1+\cos\left(\frac{\pi y}{b}\right)\right), \tag{2}$$

where E and v are the Young's modulus and Poisson's ratio of the isotropic plate (film), and h is its thickness. The dimensionless buckling amplitude ξ depends on the ratio of the biaxial compressive stress in the unbuckled plate, σ_0, called the film stress in short, to its value at the onset of buckling according to

$$\xi \equiv \left(\frac{w_{\max}}{h}\right) = \sqrt{\frac{4}{3}\left(\frac{\sigma_0}{\sigma_C}-1\right)}. \tag{3}$$

For a given film stress, σ_0, it is useful to define the half-width, b_0, associated with the onset of bucking, which is given by (1) with $\sigma_C = \sigma_0$: i.e.

$$b_0 = \frac{\pi h}{2\sqrt{3}}\sqrt{\frac{E}{(1-v^2)\sigma_0}}. \tag{4}$$

It follows that

$$\frac{\sigma_0}{\sigma_C} = \left(\frac{b}{b_0}\right)^2, \tag{5}$$

and thus the stress ratio σ_0/σ_C is directly related to the ratio of the delamination width to the minimum width for buckling.

The Euler mode has been used to compute the energy release rate along the sides of the buckle, but here the focus is on the energy release rate $\bar{G}$ averaged over the curved end of the interface delamination crack propagating along the strip. For a strip of low adhesion of width $2b$, steady-state conditions at the propagating end prevail once the buckle delamination is several times longer than its width. The average energy release rate is simply the difference between the energy per area in the plate, U_0, ahead of the propagating end (in the unbuckled state) and the average energy per unit area well behind the end in the buckled state, $\bar{U}$, i.e. $\bar{G} = U_0 - \bar{U}$. The energy per area in the unbuckled state of equi-biaxial compression is

$$U_0 = \frac{(1-v)\sigma_0^2 h}{E}, \tag{6}$$

while the average energy per area in the buckled state is found using (1)–(3) to be [10]

$$\bar{U} = U_0\left(1-\left(\frac{1+v}{2}\right)\left(1-\frac{\sigma_C}{\sigma_0}\right)^2\right). \tag{7}$$

The energy release rate for the Euler mode is [10]

$$\bar{G} = G_0\left(1-\frac{\sigma_C}{\sigma_0}\right)^2, \tag{8}$$

where G_0 is the available energy per area stored in the unbuckled film subject to release under plane strain conditions (e.g. with no strain change parallel to the crack front):

$$G_0 = \frac{1+v}{2}U_0 = \frac{(1-v^2)\sigma_0^2 h}{2E}. \tag{9}$$

Plots of $\bar{U}/U_0$ and $\bar{G}/U_0$ for the Euler mode are included in Figs. 7 and 8, which will be introduced later when the corresponding results for the two other morphologies are discussed in the next sub-section.

3.2. Post-buckling energy and energy release rate for the undulating modes

The Euler mode releases compression in the y-direction, but not in the x-direction. When σ_0/σ_C becomes large, axial undulations are able to reduce compression in the x-direction thereby further lowering the energy in the buckled state; the Euler mode becomes unstable and undergoes bifurcation into a mode with axial undulations. Bifurcation from the Euler mode takes place in a mode with normal deflection in the form $w = f(y)\cos(2\pi x/\ell)$, where $f(y)$ is either symmetric or anti-symmetric about $y = 0$ [11,13]. The plot of σ_0/σ_C, b/b_0 and $\ell/2b$ at bifurcation is shown in Fig. 5, depending only on Poisson's ratio v [13]. For $v = 0.3$, corresponding to the value used in the numerical calculations in this paper, the Euler mode bifurcates into an unsymmetric undulating mode (an incipient telephone cord mode) at $\sigma_0/\sigma_C = 6.5$ (or, equivalently, at $b/b_0 = 2.5$) with $\ell/b = 0.96$. If $v < 0.25$, the mode associated with the lowest bifurcation stress is symmetric (an incipient varicose mode).

Determination of deformation and energy at film stresses exceeding the bifurcation stress for the plate buckled in either the telephone cord mode or the symmetric varicose mode (see Fig. 4) requires numerical analysis of highly nonlinear deformation. We have performed a series of numerical calculations reported below using the finite element code, ABAQUS [15]. Quadratic thin shell elements with 5 degrees of freedom at each node and with reduced integration are used. The grid in Fig. 4 is attached to rigid substrate outside the

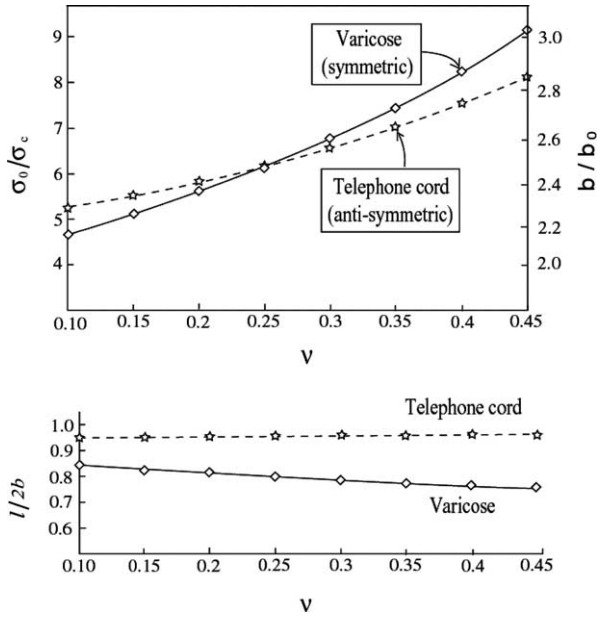

Fig. 5. Stress, half-width and undulation wavelength as a function of Poisson's ratio associated with bifurcation from the Euler mode for an infinite plate of width $2b$ clamped along its edges and subject to equi-biaxial compression σ_0 in the unbuckled state from Audoly [13]. Symmetric and anti-symmetric bifurcation modes about the centerline exist.

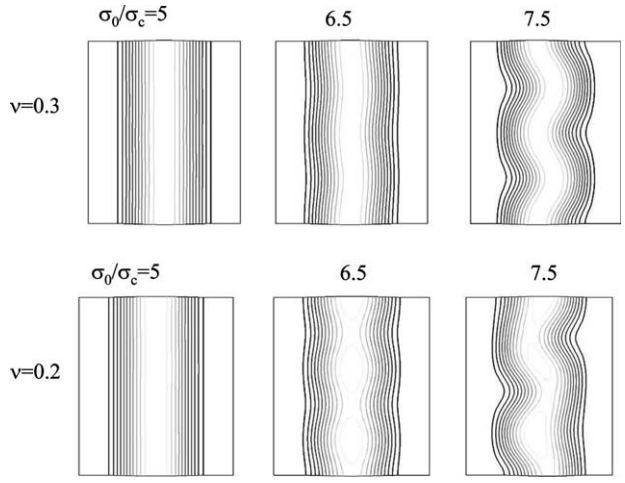

Fig. 6. Contour plots of the normal deflection of the clamped plate at three values of film stress for two values of Poisson's ratios (see Fig. 5 for the basis of the choices). The Euler mode is in effect for $\sigma_0/\sigma_C = 5$, the varicose mode or an incipient telephone cord mode can been seen at $\sigma_0/\sigma_C = 6.5$, depending on Poisson's ratio, and a telephone cord-like mode is evident at $\sigma_0/\sigma_C = 7.5$. Computed with $L/2b = 0.96$.

strip for $|y| > b$. Symmetry boundary conditions are applied at $x = 0$ and $x = L$. Calculations are repeated for various L/b to determine the wavelength ratio ℓ/b associated with the minimum energy state. For analyzing the varicose mode, symmetry conditions are imposed along $y = 0$ and only half of the grid shown in Fig. 4 is used; unsymmetric modes are thereby excluded. The entire grid is used for analyzing the telephone cord mode. Very small geometric initial imperfections are used to trigger deflections in the various modes. The imperfection is a perturbation of the initial nodal points of the middle surface of the plate by a tiny fraction of the plate thickness. Once a mode has formed, its shape is virtually independent of details of imperfection since the imperfection amplitude is so small. The buckles in Fig. 4 are representative of the three kinds of modes.

Fig. 6 illustrates the progression under increasing film stress from Euler mode to undulating mode for $\nu = 0.2$ and 0.3. In each of these examples, the initial imperfection has both symmetric and anti-symmetric components such that either undulating mode can be triggered. For $\nu = 0.3$, the Euler mode gives way directly to the telephone cord mode as σ_0/σ_C increases above the bifurcation stress. Asymmetry is just beginning to emerge at $\sigma_0/\sigma_C = 6.5$, promoted by the initial imperfection. On the other hand, if $\nu = 0.2$, the symmetric varicose mode is evident at stresses just above the bifurcation point, consistent with the bifurcation results in Fig. 5. However, the varicose mode gives way almost immediately a non-symmetric, mode with features similar to those of the telephone cord mode as the film stress is further increased. Significantly, the present nonlinear analysis reveals that the "window of conditions" for the existence of the symmetric varicose mode is exceptionally narrow, consistent with the fact that varicose modes are hardly ever observed experimentally under equi-biaxial film stress states unless they are artificially induced. For an imperfection-free system, the present results make it suggest that bifurcation from the symmetric varicose mode into an unsymmetric telephone cord-like mode occurs at a stress slightly above $\sigma_0/\sigma_C = 6.5$, although the relevant bifurcation analysis to establish this assertion has not been carried out.

The elastic strain energy in the buckled plate is averaged over the grid to give $\bar{U}/U_0$ as a function of σ_0/σ_C for each value of ℓ/b. A large number of computed results are presented in Fig. 7(a) for $\nu = 0.3$ with the objective of identifying minimum energy states. Over the range of σ_0/σ_C for which these results are presented, no contact occurs between the buckled plate and the substrate. The numerical results for the Euler mode (enforcing symmetry with no x-dependence) provide a check on the accuracy of the finite element results – excellent agreement between the numerical results and the exact result (8) is evident. For $\sigma_0/\sigma_C > 6.5$, the lowest energy in the buckled state is that associated with the telephone cord mode. The minimum of $\bar{U}$ with respect to $\ell/2b$ is very shallow for both undulation modes. We have not attempted to refine the search for the minimum beyond what is shown in Fig. 7(a). It appears that even at film stress well above $\sigma_0/\sigma_C = 6.5$ the wavelength associated with the minimum energy state

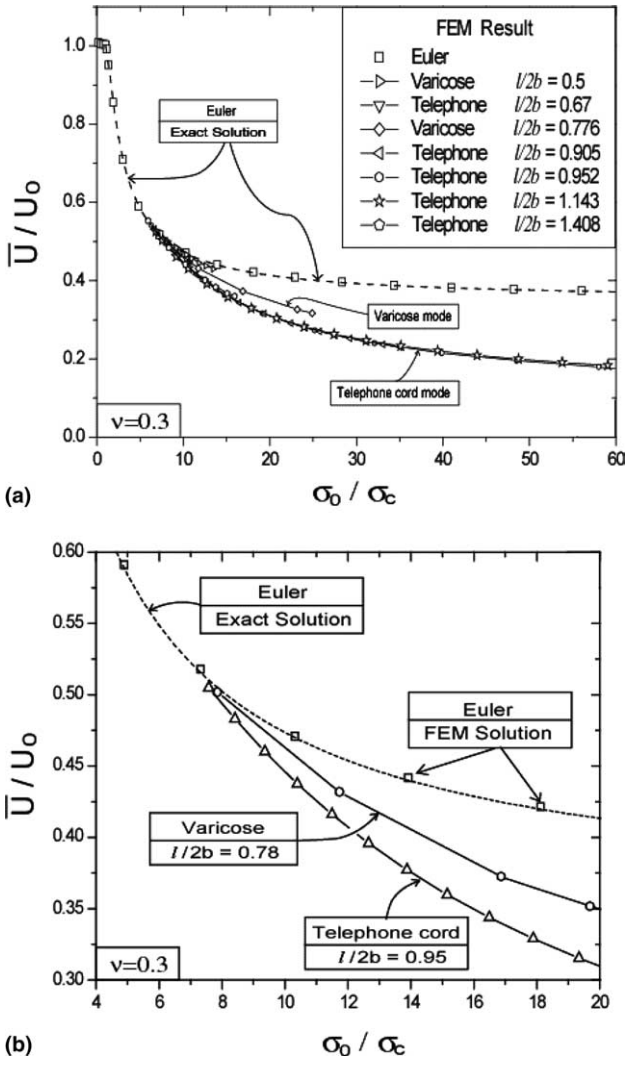

Fig. 7. Ratio of the average energy per unit area in the buckled state to that in the unbuckled state, $\bar{U}/U_0$, as a function of σ_0/σ_C for $\nu = 0.3$ for three modes: the Euler mode, the symmetric varicose mode, and the asymmetric telephone cord mode. In (a), results for various wavelengths, $\ell/2b$, are shown for the two undulating modes. In (b), results are given for the wavelength associated with bifurcation. Only the Euler mode exists for $\sigma_0/\sigma_C < 6.5$. Only the telephone cord mode is stable for $\sigma_0/\sigma_C > 6.5$. The exact result for the Euler mode is given by (8).

can be taken as a good approximation as the critical wavelength in Fig. 5 associated with the bifurcation mode. Fig. 7(b) presents the minimum energy per unit area for the each of the three modes in the range $4 < \sigma_0/\sigma_C < 20$ computed using the critical wavelengths associated with bifurcation. The energy of the varicose mode falls roughly halfway between that of the Euler mode and the telephone cord mode. As noted earlier the varicose mode, like the Euler mode, is almost certainly unstable with respect to unsymmetric deformations when $\sigma_0/\sigma_C > 6.5$ with $\nu > 0.25$. The telephone cord is the mode likely to be observed for $\sigma_0/\sigma_C > 6.5$ or, equivalently, for $b/b_0 > 2.5$.

For each of the three modes, the normalized average energy release rate $\bar{G}/U_0$ is plotted in Fig. 8(a) based on the relation $\bar{G} = U_0 - \bar{U}$ or $\bar{G}/U_0 = 1 - \bar{U}/U_0$ for $\nu = 0.3$. The relation (8) for the Euler mode holds for $\sigma_0/\sigma_C < 6.5$ (or, equivalently, $b/b_0 < 2.5$) while the maximum energy release rate for $\sigma_0/\sigma_C > 6.5$ is associated with the telephone cord mode. For the telephone and varicose modes, $\bar{G}$ is the energy release rate averaged over one complete wavelength of propagation. We speculate that $\bar{G}$ will asymptotically approach the elastic energy per area stored in the unbuckled film, U_0, as $\sigma_0/\sigma_C \to \infty$, but $\bar{G}/U_0$ has only attained 0.75 for $\sigma_0/\sigma_C = 30$. Note, however, that the telephone cord energy release rate $\bar{G}$ exceeds the available energy per area subject to plane strain constraint, $G_0 = (1+\nu)U_0/2$, which is the asymptotic limit for the Euler mode. Results for $\bar{G}/U_0$ for the Euler mode and the telephone cord mode are presented in Fig. 8(b) for various Poisson's ratio values, showing that this normalization $\bar{G}/U_0$ for the telephone cord mode is relatively independent of Poisson's ratio at large values of σ_0/σ_C.

Once nucleated, the condition for the buckle delamination to propagate along the strip is

$$\bar{G} \geqslant \Gamma_C. \tag{10}$$

The interface toughness, Γ_C, depends on the relative proportion of the mode II to mode I stress intensity factors acting on the propagating interface crack front [10]. Methods to estimate the mode mix for buckle delaminations are presented in [3]. For an equi-biaxial compressive film stress σ_0, such as applies in Fig. 1, the implication of (10) is that very narrow strips with $\bar{G} < \Gamma_C$ will not delaminate. However, for wider strips with $\bar{G} > \Gamma_C$, buckle delaminations will propagate unimpeded (dynamically) along the strip once nucleated. Patterning strips of various widths provides a method to bracket the interface toughness relevant to buckle delamination. *The toughness measured is that of the modified strip interface.* For the technique to be employed for measuring toughness of a given film/substrate interface, the patterning procedure would have modified so as to enhance adhesion outside the strips without altering adhesion within the strip. This should be viable, at least for some interfaces, and will be pursued in subsequent work.

The DLC film on the silicon substrate in Fig. 1 nicely illustrates the method of bracketing Γ_C mentioned above for the strip interface. Based on the measurement techniques noted above, the DLC film in Figs. 1 and 2 is characterized by

$$h = 0.26\ \mu\text{m}, \quad \sigma_0 = 1.4\ \text{GPa}, \quad E = 100\ \text{GPa}, \quad \nu \approx 0.3. \tag{11}$$

By (4), (6) and (9),

$$b_0 = 2.1\ \mu\text{m}, \quad U_0 = 3.57\ \text{J m}^{-2}, \quad G_0 = 2.32\ \text{J m}^{-2}. \tag{12}$$

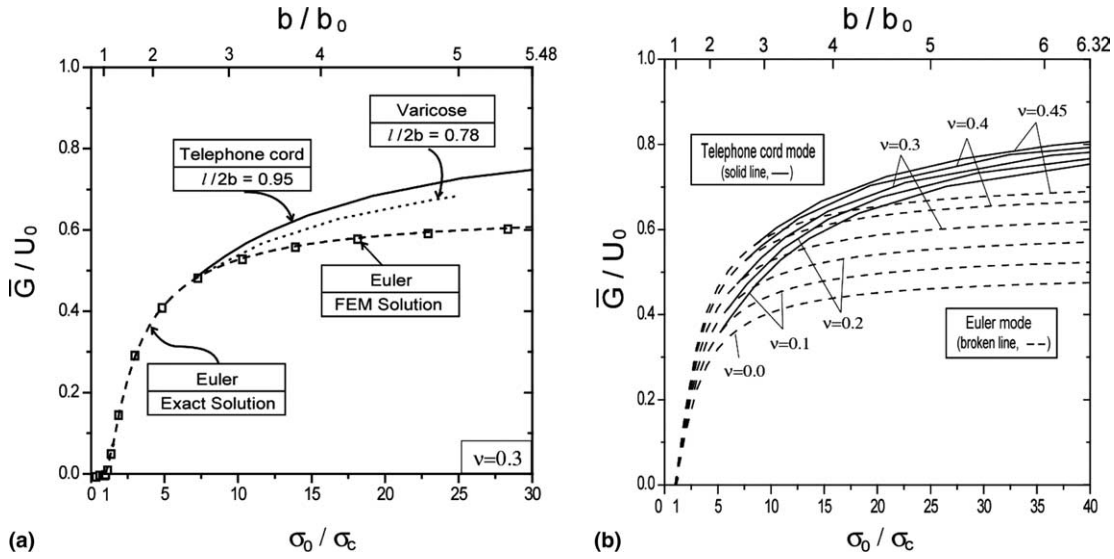

Fig. 8. (a) Normalized average energy release rate for buckle delamination along a straight-sided strip, $\bar{G}/U_0$, for each of the three buckle morphologies as a function of σ_0/σ_C and b/b_0 for $\nu = 0.3$. The film is in equi-biaxial compression, σ_0, in the unbuckled state. (b) The role of Poisson's ratio on the normalized average energy release rate for buckle delamination along a straight-sided strip, $\bar{G}/U_0$, for the Euler mode and the telephone cord mode as a function of σ_0/σ_C and b/b_0. The film is in equi-biaxial compression, σ_0, in the unbuckled state.

The width of the widest strip in Fig. 1 that did not delaminate is $2b = 6$ μm, which by (8) corresponds to $\bar{G} = 0.61\ \mathrm{J\,m^{-2}}$ had delamination occurred.[1] The width of the narrowest strip that did delaminate (in the Euler mode) is $2b = 8$ μm, corresponding to $\bar{G} = 1.23\ \mathrm{J\,m^{-2}}$. Thus, the interface toughness governing the buckling delamination is bracketed by

$$0.61\ \mathrm{J\,m^{-2}} < \Gamma_C < 1.23\ \mathrm{J\,m^{-2}}. \tag{13}$$

A more refined determination is afforded by delamination along a tapered strip.

4. Buckle delamination propagation along a tapered strip of low adhesion

4.1. Experimental observation and measurement of Γ_C

The patterning process has been employed to create a gradually tapered strip of low interface adhesion. When a buckle delamination is nucleated at the wide end of the strip (by an indenter, for example), the delamination propagates along the strip toward the narrow end, first as a telephone cord mode and then as an Euler mode as the strip narrows until it arrests when the strip becomes so narrow that $\bar{G}$ drops below Γ_C. An example has been presented in Fig. 2 for the modified DLC/silicon system characterized by (11) and (12). An atomic force microscope has been used to trace the profile of the buckle in Fig. 2 at various points along its length. At a point just to the left of the arrested end where the Euler mode is in effect, the width is $2b = 6.9$ μm and the amplitude of the buckle deflection is measured as $w_{\max} = 427$ nm. The gradual taper of the strip in Fig. 2 permits results from the previous section for the constant width strips can be used to estimate $\bar{G}$ as a function of the width at any point along the strip. Just to the left of the arrested end, $\sigma_0/\sigma_C = (b/b_0)^2 = 2.72$. Thus, based on the result (8) for the Euler mode, $\bar{G} = 0.93\ \mathrm{J\,m^{-2}}$ at arrest. Identification of the interface toughness with the energy release rate at arrest gives $\Gamma_C = 0.93\ \mathrm{J\,m^{-2}}$. This value, which indeed falls between the brackets determined in the previous section, should be an accurate measurement of the toughness of the patterned interface under the mode mix relevant to buckle delamination.

It should be noted that the propagation condition (10) is necessary but not sufficient in the sense that the fracture condition is not enforced pointwise along the curved front of the delamination, but only as an average over the propagating front. If there is a significant variation of the mode mix from point to point on the propagating crack front, identification of Γ_C with $\bar{G}$ produces the corresponding average of the interface toughness over the crack front. Pointwise estimation of the energy release rate and mode mix along the edge of a telephone cord delamination has been used to determine the interface toughness and associated mode mix of a Pt/SiO_2 interface [16]. The method was used to systematically explore the relation between one of the variables in the film deposition process and the interface toughness.

[1] The strip is wide enough to buckle had interface separation occurred since $b > b_0$. The reason delamination does not occur is that insufficient energy is made available by interface separation, i.e. $\bar{G} < \Gamma_C$.

The theoretical prediction for the buckle amplitude from (2), i.e. $\xi = w_{\max}/h = 1.52$ or $w_{\max} = 394$ nm, compares favorably with the experimental measurement, $w_{\max} = 427$ nm. Another comparison between theory and features of the observed mode shape is given in Fig. 9 where measured values of the width and wavelength of the telephone cord mode are plotted. The measurements are taken from both gradually tapered strips and straight-sided strips. The points all lie above the bifurcation line marking the transition between the Euler mode and the telephone cord mode. Many of the measured wavelengths fall very near the critical wavelength associated with bifurcation. However, some wavelengths are as much 40% above the critical wavelength, most likely reflecting the shallowness of the minimum energy state with respect to $\ell/2b$ seen in Fig. 7(a).

4.2. Numerical simulation of buckle pattern

As in all the cases considered in this paper, the unbuckled plate is subject to the equi-biaxial compressive stress σ_0, and the reference half-width associated with incipient buckling, b_0, is defined in (4). The finite element program has been applied to analyze several tapered plates clamped along their edges. The example in Fig. 10 has a width $4.3b_0$ at the top and approximately b_0 at the bottom. Along the top and bottom edges, the plate is constrained to undergo no displace in the lengthwise direction or rotation about the edgewise direction, but it is unconstrained in the normal and tangential directions (analogous to symmetry boundary conditions). The essential aspects of the buckling behavior are insensitive to the boundary conditions imposed on the top and bottom edges everywhere but near those edges. Points along the length

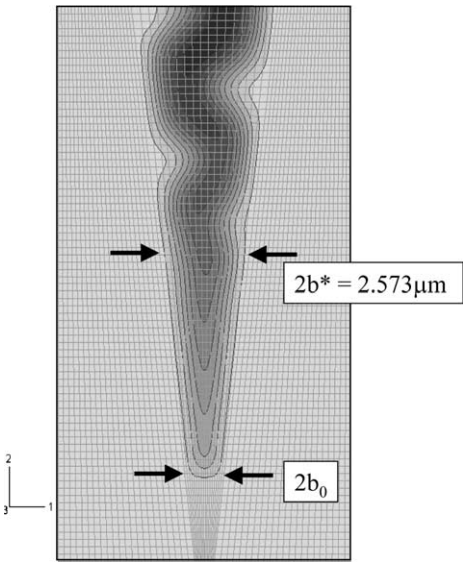

Fig. 10. Contour plot of the normal deflection of a tapered clamped plate as predicted by a finite element analysis for $v = 0.3$. The transition from asymmetric telephone cord mode to the symmetric Euler mode occurs very near the width associated with bifurcation for the straight-sided plate. The deflection becomes almost zero where the width drops below $2b_0$, corresponding to the minimum width for buckling of a straight-sided plate.

of the plate corresponding to widths $2b_0$ and $2b_*$ are marked in Fig. 10, where (for $v = 0.3$) $b_* = 2.5b_0$ is the half-width of the straight-sided clamped plate associated with bifurcation of the Euler mode into the telephone cord mode. Even though the taper in this example is not as gradual as in the experimental case, the transition from the telephone cord morphology to the Euler mode occurs very near where the width is $2b_*$. Moreover, the buckle amplitude vanishes in the region of the plate where the width drops below $2b_0$. As in the computations reported in Section 3, a contact

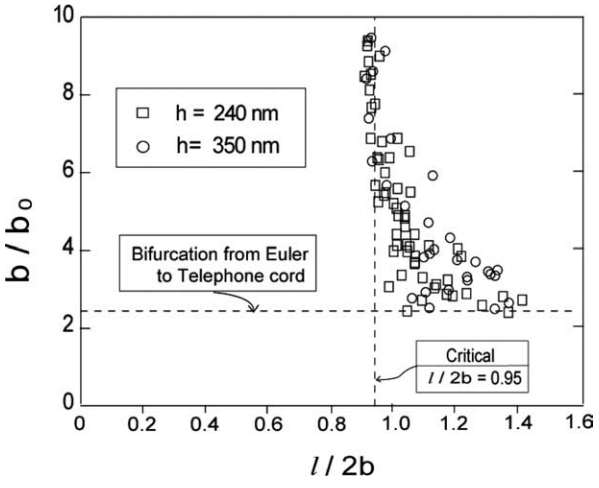

Fig. 9. Experimentally measured half-width and wavelength for various telephone cord modes for the DLC/silicon system for two values of film thickness.

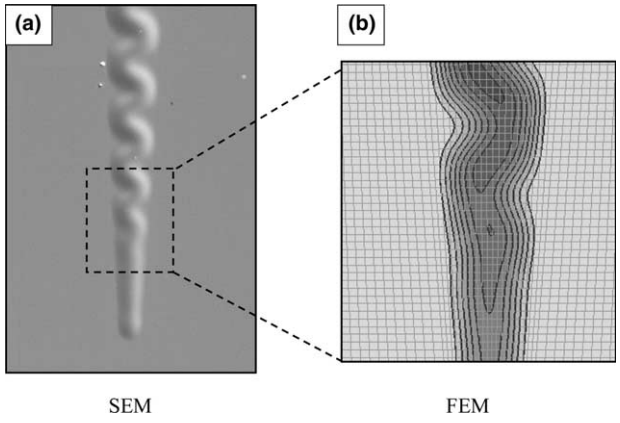

Fig. 11. Comparison of an SEM image of a DLC/silicon buckle with a finite element simulation in the transition region between modes. The film stress, geometry and properties of the film in (a) are used in the simulation in (b).

constraint between the plate and the substrate need not be invoked since no contact of plate and substrate occurs in the solution.

A second example is shown in Fig. 11 where a finite element simulation has been performed to model a section of an experimentally observed transition between the telephone cord and Euler morphologies. Here, the thickness, tapered width, modulus and pre-buckling stress in the plate have all been taken to be the same as in the DLC film, and the computed buckle pattern is shown side-by-side with the observed pattern.

5. Closing remarks

Techniques have been described for creating regions of low adhesion whose boundaries confine buckle delaminations. Highly controlled buckle delamination patterns can be achieved. In this paper, films subject to equi-biaxial compression in the unbuckled state have been considered. For low adhesion regions that are straight-sided strips, the width and film stress determine the morphology of the buckle mode. The smooth Euler mode is dominant for $1 < \sigma_0/\sigma_C < 6.5$, giving way to an undulating mode very similar to the telephone cord mode for $\sigma_0/\sigma_C > 6.5$. Interpretation of these results is aided by the identity, $\sigma_0/\sigma_C = (b/b_0)^2$, where b_0 defined in (4) is the half width of a strip that will just begin to buckle at the film stress σ_0. A symmetric undulating varicose mode is expected only in a narrow range of stresses (or widths) when $\nu < 0.25$.

Average energy release rates governing interface delamination are presented for all the modes. For $\sigma_0/\sigma_C > 6.5$, the telephone cord mode releases more energy per area of delaminated interface than the Euler mode (or the varicose mode), as summarized in Fig. 8, and only the telephone cord morphology is stable in this range. The width of a gradually tapered strip at the point of delamination arrest can be used to infer the interface toughness of the strip interface. In the present study, the patterning process reduces the toughness of strip interface. If the method is to be an effective means of measuring interface toughness, the process would have to modify the interface outside the strip by increasing its toughness.

A wide variety of buckle delamination patterns can be achieved. It is possible to lay down grids or networks of channels with openings several microns wide and height as small as a fraction of a micron. Such channel may have potential as micro-fluidic networks since they can be created with sub-micron openings. The cross-sectional area of the channel for the Euler mode is

$$A = bh\sqrt{\frac{4}{3}\left[\left(\frac{b}{b_0}\right)^2 - 1\right]}. \tag{14}$$

The amplitude of the open channel between the film and substrate can be adjusted by changing either the film stress or the strip width, cf. Eq. (3). For example, local heating of the DLC film will cause it to expand relative to the substrate, thereby relaxing the compressive film stress and decreasing the channel opening at a specific location along its length. Future work will explore the scope of such grids and networks of channels.

Acknowledgements

The work of KRL and MWM at KIST was financially supported by the Center for Nanostructured Materials Technology under the 21st Century Frontier R&D Program of the Ministry of Science and Technology, Korea. In addition, the work of MWM was partially supported by a grant from BK21, and the work of JWH was supported in part by Grant NSF DMR 0213805 and in part by the Division of Engineering and Applied Sciences, Harvard University.

References

[1] Thouless MD. J Am Ceram Soc 1993;76(11):2936.
[2] Gille G, Bau B. Thin Solid Films 1984;120:109.
[3] Moon M-W, Jensen HM, Oh KH, Hutchinson JW, Evans AG. J Mech Phys Solids 2002;50(11):2355.
[4] Hutchinson JW, Thouless MD, Liniger EG. Acta Metall Mater 1992;40(2):295.
[5] Volinsky AA. Mater Res Soc Symp Proc 2003;749:W10.7.
[6] Moon M-W, Chung J-W, Lee K-R, Oh KH, Wang R, Evans AG. Acta Mater 2002;50:1219.
[7] Cho S-J, Lee K-R, Eun KY, Jeong J-H, Kwon D. Diamond Rel Mater 1999;8:1067.
[8] Yu HH, Hutchinson JW. Int J Fract 2002;113:39.
[9] Cotterell B, Chen Z. Int J Fract 2000;104:169.
[10] Hutchinson JW, Suo Z. Adv Appl Mech 1992;29:63.
[11] Jensen HM. Acta Metal Mater 1993;41:601.
[12] Jensen HM, Sheinman I. Int J Fract 2001;110:371.
[13] Audoly B. Phys Rev Lett 1999;83(20):4124.
[14] Audoly B, Roman B, Pocheau A. Eur Phys J B 2002;27:7.
[15] Hibbit, Karlsson & Sorensen Inc. ABAQUS version 6.3 user's manual, 2003. Hibbit, Karlsson & Sorensen Inc., Pawtucket, RI.
[16] Lee A, Clemens BM, Nix WD. Acta Mater 2004;52(7):2081.